Elsevier Editorial System(tm) for Journal of Hydrology

Manuscript Draft

Manuscript Number: HYDROL24569R2

Title: Identifying seawater intrusion in coastal areas by means of 1D and quasi-2D joint inversion of TDEM and VES data

Article Type: Research paper

Keywords: coastal aquifers; seawater intrusion; joint inversion; lateral constrained; drilling exploration.

Corresponding Author: Dr. Francisco José Martínez-Moreno, Ph.D.

Corresponding Author's Institution: University of Lisbon

First Author: Francisco José Martínez-Moreno, Ph.D.

Order of Authors: Francisco José Martínez-Moreno, Ph.D.; Fernando A. Monteiro-Santos, Professor; Ivo Bernardo; Mohammad Farzamian, Ph.D; Catarina Nascimento; Judite Fernandes, Ph.D.; Bruno Casal; Joana Ribeiro, Ph.D. student

Abstract: Seawater intrusion is an increasingly widespread problem in coastal aquifers caused by climate changes -sea-level rise, extreme phenomena like flooding and droughts- and groundwater depletion near to the coastline. To evaluate and mitigate the environmental risks of this phenomenon it is necessary to characterize the coastal aquifer and the salt intrusion. Geophysical methods are the most appropriate tool to address these researches. Among all geophysical techniques, electrical methods are able to detect seawater intrusions due to the high resistivity contrast between saltwater, freshwater and geological layers. The combination of two or more geophysical methods is recommended and they are more efficient when both data are inverted jointly because the final model encompasses the physical properties measured for each methods. In this investigation, joint inversion of vertical electric and time domain soundings has been performed to examine seawater intrusion in an area within the Ferragudo-Albufeira aquifer system (Algarve, South of Portugal). For this purpose two profiles combining electrical resistivity tomography (ERT) and time domain electromagnetic (TDEM) methods were measured and the results were compared with the information obtained from exploration drilling. Three different inversions have been carried out: single inversion of the ERT and TDEM data, 1D joint inversion and quasi-2D joint inversion. Single inversion results identify seawater intrusion, although the sedimentary layers detected in exploration drilling were not well differentiated. The models obtained with 1D joint inversion improve the previous inversion due to better detection of sedimentary layer and the seawater intrusion appear to be better defined. Finally, the quasi-2D joint inversion reveals a more realistic shape of the seawater intrusion and it is able to distinguish more sedimentary layers recognised in the exploration drilling. This study demonstrates that the quasi-2D joint inversion improves the previous inversions methods making it a powerful tool applicable to different research areas.

Response to Reviewers:

Identifying seawater intrusion in coastal areas by means of 1D and quasi–2D joint inversion of TDEM and VES data

F.J. Martínez-Moreno[a*], F.A. Monteiro-Santos[a], I. Bernardo[a], M. Farzamian[a], C. Nascimento[a], J. Fernandes[b], B. Casal[c], J.A. Ribeiro[a]

[a] Instituto Dom Luiz, Universidade de Lisboa, Faculdade de Ciências, Campo Grande, Edif. C8, Lisboa, Portugal.

[b] LNEG, National Laboratory of Energy and Geology, Estrada do Zambujal, Apartado 7586, 2721-866 Alfragide, Portugal.

[c] Sondagens Casal, Lda., Estrada do Moinho, 2705-432, São João das Lampas, Areias, Portugal.

*Corresponding author e-mail: fjmoreno@fc.ul.pt

ABSTRACT

Seawater intrusion is an increasingly widespread problem in coastal aquifers caused by climate changes –sea-level rise, extreme phenomena like flooding and droughts– and groundwater depletion near to the coastline. To evaluate and mitigate the environmental risks of this phenomenon it is necessary to characterize the coastal aquifer and the salt intrusion. Geophysical methods are the most appropriate tool to address these researches. Among all geophysical techniques, electrical methods are able to detect seawater intrusions due to the high resistivity contrast between saltwater, freshwater and geological layers. The combination of two or more geophysical methods is recommended and they are more efficient when both data are inverted jointly because the final model encompasses the physical properties measured for each methods. In this investigation, joint inversion of vertical electric and time domain soundings has been performed to examine seawater intrusion in an area within the Ferragudo-Albufeira aquifer system (Algarve, South of Portugal). For this purpose two profiles combining electrical resistivity tomography (ERT) and time domain electromagnetic (TDEM) methods were measured and the results were compared with the information obtained from exploration drilling. Three different inversions have been carried out: single inversion of the ERT and TDEM data, 1D joint inversion and quasi-2D joint inversion. Single inversion results identify seawater intrusion, although the sedimentary layers detected in exploration drilling were not well differentiated. The models obtained with 1D joint inversion improve the previous inversion due to better detection of sedimentary layer and the seawater intrusion appear to be better defined. Finally, the quasi-2D joint inversion reveals a more realistic shape of the seawater intrusion and it is able to distinguish more sedimentary layers recognised in the exploration drilling. This study demonstrates that the quasi-2D joint inversion improves the previous inversions methods making it a powerful tool applicable to different research areas.

Keywords: coastal aquifers, seawater intrusion, joint inversion, lateral constrained, drilling exploration.

Highlights

- Seawater intrusion is an increasingly problem in coastal aquifers.
- Electrical and electromagnetic methods are combined to detect seawater intrusion.
- Traditional single data inversion detects such intrusion with uncertainties.
- 1D joint inversion improves the single data inversion and distinguish more layers.
- Quasi–2D inversion better defines geology and seawater intrusion.

1. Introduction

Coastal aquifers constitute the major water reservoir for freshwater supply in many countries, mainly in arid and semiarid zones (Bear *et al.*, 1999). However, freshwater belonging to these type of aquifers is susceptible to be degraded due to its proximity to seawater. Together with the high intensive water demands caused by higher population densities in coastal areas (Werner *et al.*, 2013), this can lead to the process known as 'Seawater Intrusion' (Werner and Gallagher, 2006). This phenomenon is defined as landward incursion of seawater caused by both natural and anthropogenic processes. Sea-level rise associated with climate changes –changes of atmospheric pressure, melting of ice sheets and glaciers, expansions of oceans and seas as they warm, etc.– (Sherif and Singh 1999) and anthropogenic influences such as groundwater depletion near to the coastal line or land uses changes, among others (Custodio, 1987) are the main causes of seawater intrusions and, therefore, reduction in the available freshwater storage volume and aquifer contamination.

Detecting seawater intrusion in local areas is the first stage for the problem remediation (Duque *et al.*, 2008; Nguyen *et al.*, 2009). Direct observation made into drill-holes allow to evaluate the seawater intrusion in an area (Calvache and Pulido-Bosch, 1994), however it depends on a suitable drilling holes distribution to obtain accurate results. Otherwise, this procedure only provides partial information about the seawater intrusion. Geophysical methods provide a more general approach to the problem (Abdul Nassir *et al.*, 2000) where electrical resistivity techniques are the most appropriate due to the high resistivity contrast between fresh and salt water (Khalil *et al.*, 2013; El-Kaliouby and Abdalla, 2015).

Time Domain Electromagnetic (TDEM) provides 1D underground resistivity variation and it is able to determine groundwater distribution in a specific area

(Martinez-Moreno *et al.*, 2016). The presence of fresh or salt water produces a sudden change in resistivity from high values (in unsaturated rocks) to low (freshwater) or very low (saltwater) values. Geoelectrical methods such as electrical resistivity tomography (ERT) offers a 2D pseudosection underlining the resistivity distribution underground (Kazakis *et al.*, 2016). For example, Sherif *et al.* (2006) compare ERT results with hydrochemical parameters to evaluate seawater intrusion. Classical methods as Vertical Electrical Soundings (VES) have been widely used for detection of saltwater intrusion (Song *et al.*, 2007; Adepelumi *et al.*, 2009). The VES is useful to determine saltwater intrusion accurately in predominant layered media.

The application of both techniques combined (TDEM and ERT) is widely used in mining, geotechnical, hydrogeological and environmental studies (Meju, 2002; Nicaise *et al.*, 2013). The TDEM method can accurately indicates conductive structures and it can easily have a major depth of investigation. In turn, the resistivity profiles defines better resistive areas and it better underlines shallow structures (Monteiro Santos and El-Kaliouby, 2011). Thus, both methods are complementary and can offer more accurately results.

While the ERT method is usually interpreted in 2D or 3D arrays, interpretation of TDEM data generally is done assuming 1D models due to its computation is difficult and time-consuming even in forward modelling (Monteiro-Santos and El-Kaliouby, 2011). A joint inversion of DRC and TDEM data can help reduce uncertainties and ambiguities to interpret the obtained results. Vozoff and Jupp (1975) were pioneers in joint inversion of magnetotelluric (MT) and vertical electrical soundings (VES) methods. Since then, joint inversion applied to different geophysical techniques has been employed: Monteiro Santos *et al.*, 1997; Schmutz *et al.*, 2000; Monteiro-Santos and El-Kaliouby, 2010.

Classical joint inversions of TDEM and resistivity data use a single 1D geophysical model for each sounding and finally obtain an interpolated 2D-pseudosection (Schmutz *et al.*, 2000; Monteiro-Santos and El-Kaliouby, 2011). However, this approach can produce models with abrupt lateral variations due to noise, equivalence problems and 2D-3D effects (Viezolli *et al.*, 2008). Such effects can be reduced using a laterally constrained inversion (LCI) (Auken and Christiansen, 2004; Monteiro-Santos, 2004; Auken *et al.*, 2005). This algorithm allows constraining parameters during the inversion in order to obtain a model with a smooth lateral variation.

This research aims to detect seawater intrusion by comparing the results obtained in electrical resistivity and TDEM techniques in different situations: single inversion, 1D and quasi-2D joint inversions. The obtained models for each inversion will be compared to the information obtained in the exploration drilling performed in the study area.

2. Geological framework

The study area is located in Algarve region (South of Portugal, Fig. 1) between the towns of Ferragudo and Albufeira. From the standpoint of regional geological context, the area fits in Meso-Cenozoic Basin, a major tectonostratigrafic zone of the Iberian Peninsula, at the southern portion of the South Portuguese zone (Simancas, 2004).

The onshore Meso-Cenozoic Algarve Basin consists in an E-W trending sedimentary basin filled by more than 4000 m of sediment deposited on Carboniferous schists and greywackes (Lopes *et al.*, 2006). Sandstones and conglomerates belonging to the '*Arenitos de Silves*' are deposited discordantly on the paleozoic substratum during the middle to upper Triassic, followed by the '*Complexo Pelítico Carbonatado-Evaporítico*' (Francés *et al.*, 2014). A volcanic-sedimentary complex related to the first rifting phase (Manuppella, 1992) composes the top of the sequence. This sequence includes the carboniferous formations that constitute an impermeable substratum.

The sedimentary sequence regarding to the study area is composed, from bottom to top, by: limestones at the base (Middle Jurassic); a multilayer sequence of silicate sands, limestones and silts (‘*Arenitos de Sobral*’ formation from Cretaceous; Rey, 1983); followed by alternation of limestones and marls (‘*Palorbitolina*’, Cretaceous; Rey, 1983); up to this formations were deposited carbonates from Lagos-Portimão carbonate formation (Miocene; Antunes and Pais, 1992) composed, from bottom to top by: biocalcarenites, limestones, calcareous sandstones and clays. The Faro-Quarteira formation –feldespathic sands, sandstones and clays (Quaternary) – constitutes the top of the sedimentary sequence.

From a hydrogeological point of view, the study area is located within the aquifer system of Ferragudo-Albufeira, which has an area of ~117 km^2 (Almeida *et al.*, 2000). This is a multiaquifer groundwater system where the Cretaceous and Miocene formations make up the main aquifer systems. The carbonate formation from Cretaceous (Fig. 1) creates a small karstic aquifer with high groundwater storage and quality. However, the water resource potential is low due to limited aquifer recharge by rainwater.

The Miocene aquifer is also recharged by rainwater and perhaps from the Cretaceous and Jurassic formation (see Fig. 1). At the final sections of the main streams, near the sea, there are permanent wetlands as a result of surface and groundwater discharge along these drainage axis.

3. Survey setting and method

3.1 Geophysical Profiles

In the study area (Fig. 1), electrical resistivity and Time Domain Electromagnetic (TDEM) soundings were measured along two profiles. Both geophysical methods match in space and N-S direction (Fig. 2). Profile 1 is located at the E side of the study area from the coastal line. The profile is 350 m long and it includes 6 TDEM sites slightly displaced toward the W with respect to the resistivity profile. Profile 2 is located on the W side of the study area. It is composed by a resistivity profile of 350 m long and 12 TDEM sites that exceed the extension of the resistivity profile.

At the centre of the profile 2, the exploration drilling found 16 m of sands and clays from the Quaternary, followed by 40 m of biocalcarenites, marly limestones and clays, karstified limestone and calcareous marls and clays from Miocene. At ~25 m depth were detected marly limestones and clays, in a transition zone, with a probably interstitial filling of mixed saltwater. Saltwater is located from ~30 m in depth. The electrical conductivity (EC) measured into the drill-hole were 50.1 mS/cm, whereas the seawater in the area has an EC of 55.6 mS/cm.

3.2 Resistivity profiles

Resistivity profiles were measured using the Syscal Pro 10-channels equipment (Iris, Inc.) with 4 cables segments and a maximum of 72 electrodes registering data in the same profile. The equipment introduces current in the terrain by means of a pair of steel electrodes while measuring potential differences in another pair of steel electrodes. The survey were performed using Schlumberger electrode configuration with a minimum electrode spacing of 5 m.

Several filters were applied to the raw data prior to the data inversion to exclude the noisy data: extermination of bad datum points and RMS error statistics (discarding data above 60% error, following Loke, 2016). Inverse calculation of the apparent resistivity data was carried out with the same parameters under software Res2Dinv (v. 3.59, Geotomo Inc.): least-square inversion and model refinement constraint, mesh made up of model cells and 4-nodes per unit electrode spacing.

A few vertical electrical soundings (VES) matching with the TDEM sites have been extracted from the ERT profiles in order to perform joint inversion. For that purpose, resistivity data with the appropriate AB/2 (current electrodes) and MN/2 (potential electrodes) centred at the position of the transient soundings have been selected.

3.3 Time Domain Electromagnetic

The TDEM is an inductive method based on the induction generated in the subsurface by the fast variation of the magnetic field (the primary field) originated when the current passing in a loop on the surface of the earth is cut off. A secondary magnetic field is formed by the induced currents and the receiver coil (Nabighian, 1988; Ward et al., 1990; Everett, 2013) measures its decay (dBz/dt). The apparent resistivity for late times, is calculated by,

$$\rho_a(t) = 0.125221\left(\frac{I}{u(t)}\right)^{\frac{2}{3}}\mu_0^{\frac{5}{3}}\,t^{-\frac{5}{3}}a^{\frac{8}{3}} \qquad (1)$$

Where *u(t)* is the electromotive force (*emf*) in the receiver, μ_0 the free space magnetic permeability and *a* is the current loop radius.

TDEM data was measured using the TEM-Fast48 equipment from Applied Electromagnetic Research (AEMR Inc.; Fainberg, 1999). The data was acquired in a coincident square loop configuration combining transmitter and receiver functions, with a loop of 50×50 m, a current applied of 1.9 A (profile 1) and 3.5A (profile 2). The data was processed with TEM-RES v.7.0 software from AEMR, which allows 1D modelling and inversion of the TDEM data. Prior to modelling, data spikes were removed as well as noisy early time gates due to the effects of transmitter-current contamination, and excessively noisy late time gates. The response curve of the model (relating apparent resistivity in ohm·m and time in µsec) was fitted to the observed data applying trial-error methods and automatic inversion.

3.4 Static shift and depth of investigation

Before the joint inversion, the resistivity measurements should be corrected from the static effect. The approach proposed by Meju (2005) was followed in this work; the time values of TDEM data were converted in equivalent VES AB/2 distance using the equation,

$$\boldsymbol{L} = 711.8\sqrt{\boldsymbol{t\rho}} \qquad (2)$$

where ρ is the apparent resistivity for the instant *t*.

The correction of the static shift is performed by applying a multiplicative factor to the whole resistivity curve in order to overlap both (ERT and TDEM) apparent resistivity curves (Fig. 3).

The depth of investigation (DOI) defines the limits in depth to which the results are trusted. The evaluation of the DOI and model resolution is calculated using the DOI index proposed by Oldenburg and Li (1999), which provides a model resolution including all parameters of the inverse problem, such as data and modelling error. For that purpose, two inversions were carried out applying two different initial models with resistivity values ten times higher:

$$\boldsymbol{R}_{1,2}(x,z) = \frac{\boldsymbol{m}_1(x,z) - \boldsymbol{m}_2(x,z)}{\boldsymbol{m}_{1r} - \boldsymbol{m}_{2r}} \qquad (3)$$

where m_{1r} and m_{2r} are the resistivity of the first and second reference models, and m_1

(x,z) and m_2 (x,z) are the resistivity of each cell of these models. The DOI index (R) is close to zero when the two inversions produce similar resistivity values, regardless of the reference model value. In this work it was used a cut-off value of 0.3.

3.5 1D Joint inversion

The apparent resistivity values from VES and TDEM soundings were jointly inverted assuming a 1D model and using an iterative approach based on the Levenberg-Marquardt method and Singular Value Decomposition (SVD) technique. This procedure can be seen as an optimization one where an initial model is modified until an expected misfit between data and model response is reached. The modification of the model (Δm) at iteration *k* is calculated by,

$$\left(\boldsymbol{J}(\boldsymbol{m}^k)^T\,\boldsymbol{J}(\boldsymbol{m}^k)\right)\Delta\boldsymbol{m} = -\boldsymbol{J}(\boldsymbol{m}^k)^T\boldsymbol{F}(\boldsymbol{m}^k) \tag{4}$$

where *J* indicates the Jacobian matrix, *F* represents the difference between data and model response in the logarithmic domain The system of equation is solved using the SVD technique and the Levenberg-Marquardt stabilization algorithm.

For data inversion, a software developed in FORTRAN language (Monteiro Santos and El-Kaliouby, 2010) has been used applying the method explained above. The program uses an initial model created according to the results obtained in the single inversion. Therefore, in profile 1 the initial model has 4 layers (Resistivity in ohm·m/thickness in m): 30/4, 4/10, 3.5/7, 2.5/10. In profile 2 has also been used 4 layers: 25/4, 18/12, 4/15, 3.2/4. Later, the software performs a maximum of 50 iterations for each sounding to adjust the initial model to the acquired data. Finally, it is selected the model with the lowest error.

The fitting between the curves of the model and acquired data defines the quality of the results. The selection of the best model is based on the minimum number of layers for the same adjustment quality.

3.6 Quasi-2D joint inversion

Monteiro Santos (2004) calculates 1D inversion with lateral constrained of TDEM and VES data measured with a modification of the nonlinear smoothness constrained inversion algorithm. In the inversion process, a 2D mesh of blocks is distributed according to the locations of the data (Monteiro Santos and El-Kaliouby, 2011). Calculations of VES and TDEM model responses are based on 1D forward modelling (Knight and Raiche, 1982; Raiche *et al.*, 1985).

VES and TEM calculation is performed through the convolution integral using appropriate filters. Otherwise, forward TDEM algorithm takes into account the ramp time (time the current in the transmitter takes to vanish) to calculate accurately the early time response (see more details in Monteiro Santos and El-Kaliouby, 2011).

The inverse problem requires an iterative procedure as it involves a nonlinear relationship between model response and model parameters. Logarithm of the block resistivity and apparent resistivity is used as model parameter and data set respectively. Minimization of a fitting objective function allows to estimate the correction of the model parameters for each iteration.

The objective function used in these inversions is:

$$\boldsymbol{Q} = \|\boldsymbol{W}_d(\delta\boldsymbol{d} - \boldsymbol{J}\,\delta\boldsymbol{p}\|^2 + \lambda\|\boldsymbol{C}\,(\boldsymbol{p} - \boldsymbol{p}_0)\|^2 \quad (7)$$

where ||…|| means the L_2 norm, W_d is a diagonal matrix, consisting of the reciprocal of data standard deviations, δp is the vector containing the corrections to the model parameters, and p_0 is a priori defined model. The expression $\delta d = \ln(\rho_a^c) - \ln(\rho_a^o)$ is the vector that represents the differences between apparent resistivity of the calculated model response (ρ_a^c) and the measured data (ρ_a^o). J is the derivative Jacobian matrix and

λ is a Lagrange multiplier (damping factor) used to control the balance between data fit and initial model.

The element of the matrix C are the roughness coefficients for each parameter defined for the four neighbours (upper, lower, east and west blocks). The elements of C are -4α, α or 0 for the sites into the profile, and -3α, α or 0 for the beginning and end sites of the profile. The coefficient α compensates the resolution decrease in depth of DRC and TDEM methods. Minimization of Q yields the normal equation:

$$(\mathbf{J}^T \mathbf{W}_d^T \mathbf{W}_d \mathbf{J} + \lambda \mathbf{C}^T \mathbf{C})\, \delta\mathbf{p} = \mathbf{J}^T \mathbf{W}_d^T \mathbf{W}_d\, \delta\mathbf{d} + \lambda \mathbf{C}^T \mathbf{C}\, (\mathbf{p} - \mathbf{p}_o) \quad (8)$$

Once this normal equation is solved, the model parameters are updated by adding the vector δp. The iteration process continues until the misfit is reduced to an acceptable level previously defined.

As in 1D joint inversion, a software developed in FORTRAN language (Monteiro-Santos and El-Kaliouby, 2010) has been used. A maximum of 50 iterations for each profile have been applied where it is selected the one with the lowest error. The resistivity and thickness of the initial model has been selected according to the resistivity results obtained in the TDEM and ERT profiles. The initial model for these profiles include 20 layers with thicknesses of 10 m and resistivity values ranging from 1.5 to 15 ohm.m.

4. Geophysical results

4.1 ERT and TDEM profiles

The obtained results through single inversion are shown in Fig. 4. Profile 1 of ERT (Fig. 4a) presents a shallow very resistive zone at the beginning of the profile (~1000 ohm·m (Ω·m), from 0 to 90 m long and 5 m thickness) representing the sands dunes of the study area. Beneath the resistive layer and down to 30 m depth, there are mainly sands, clays and limestones. The resistivity varies significantly in this area, revealing zones with very low resistivity (20-80 m, 120-150 m, 170-210 and 240-260 m long) less than 1 Ω·m. We anticipate that the low resistivity belonging this zone corresponds to the saltwater intrusion by means of preferential areas favouring this intrusion. In addition, there are zones with intermediate resistivity (~10 Ω·m) that is attributed to sands and clays with fresh or salty water, and finally, pointed areas (under 160 and 210 m long) with higher resistivity (~100 Ω·m) that represents limestones.

At the TDEM results (Fig. 4b) are differentiated 3 layers as follow: a shallow low resistive layer (~10 Ω·m and 10 m thickness) detecting the shallow sands, over a very low resistive layer (<2 Ω·m and 10 m thickness) and a layer at the bottom with a resistivity about 5 Ω·m. Comparing ERT and TDEM models, it is summarized that the saltwater is detected at ~10 m depth in a non-homogeneous layer regarding to DRC pseudosection.

The results obtained in profile 2 can be compared with the borehole information. The ERT profile (Fig. 4c) has a shallow layer with high resistivity (~1000 Ω·m) from 180 m length to the end, which highlights the sand dunes from the study area. Below this layer is detected an intermediate resistivity (~10 Ω·m) belonging to sands, clays, limestones and biocalcarenites. There are two zones with low resistivity under 170 (<1 Ω·m) and 250 m (~5 Ω·m) length. The area at 170 m length and 25-30 m depth highlights a very low resistivity that is attributed to clays and saltwater intrusion.

The TDEM profile (Fig. 4d) presents a 3 layers model: a shallow resistive area (500-1000 Ω·m and ~20 m thickness) that covers the whole profile belonging to the shallow sands dunes (from 180 m to the end) and clayed sands from Quaternary cover (up to 180 m long). The second layer has wedge shape from the S and a resistivity of ~5 Ω·m, and it represents the freshwater and/or a mix with salt water. At the bottom of the profile (from ~27 m depth), a low resistivity zone (below 1 Ω·m) was detected, corresponding to saltwater.

Comparing the profile 2 results with the drill-hole data it is verified that, in spite of the sediment sequence is not clearly differentiated, the saltwater is located within the karstified limestone at ~30 m depth.

4.2 1D Joint inversion

The fitting between measured and calculated data is displayed in Fig. 5. In both cases it is observed a good data adjustment between the observed and calculated data. The VES data present an error below 8% whilst the fit in TDEM data is below 3%.

Figure 6 shows the models resulting from 1D joint inversion for the two profiles. Comparing these models with the single inversion in Fig. 4, the models show an improvement were more layers are differentiated and new details are recognised. Note that the resistivity values in these models are closer to TDEM data than VES one from the single inversion due to the static shift applied to the electrical measurements.

At the resistive shallow layer in profile 1 (Fig. 6) –that presents an homogeneous resistivity of ~10 Ω·m in the single inversion in Fig. 4– it is also differentiated two high resistivity areas at the beginning and middle of the profile, with resistivity upper than 40 Ω·m. The second layer presents a better defined morphology and thickness, with a resistivity value lower than 2 Ω·m, and it is shallower at 100 m length. Finally, this profile highlights middle-high resistivity at the bottom (10-30 Ω·m) where sands, clays and limestones are located.

Profile 2 has also enhanced the morphology and the number of layers, and it presents a better fit with the drilling information. The joint inversion shows a shallow high resistive layer matching with sands and clays at a 6 m depth that represents the sand dune area. Below, there is an area with a resistivity of ~10 Ω·m belonging to sands, clays, limestones an biocalcarenites which probably highlights the fresh water saturated area. Then the third layer matching with clays, limestones and biocalcarenites has a resistivity of ~2 Ω·m representing saltwater. The bottom of the profile is marked with a resistivity lower than 2 Ω·m.

4.3 Quasi-2D joint inversion

As in the previous 1D joint inversion, this process includes lateral constraint and it has been obtained by the fitting between measured and calculated model data (Fig. 7). In this case, profile 1 presents a minor adjustment between observed data and calculated curve, and the errors are higher than in the previous inversion. However, profile 2 has a more reliable and strict data fit with lower errors.

For profile 1 (Fig. 8), results of the quasi-2D joint inversion show the same number of layers as in previous inversions: a shallow high resistive layer (upper than 20 Ω·m) over an intermediate resistive one (5-7 Ω·m), and the saltwater intrusion area is located at 10-15 m depth with a resistivity value close to 1 Ω·m. At the deeper part of the profile, below 15 m depth, it is detected a resistivity of 5-8 Ω·m. In this profile, the depth of investigation (DOI) index has been calculated to test the reliability of the results, and it is demonstrated that the whole profile has a DOI index under 0.3 –the selected cut-off value– and the model only has a not trusted area in the deeper part from the middle to the end of the profile.

Profile 2 (Fig. 8) presents more fitting and reliable results comparing with the drill-hole information. The whole profile presents a DOI index lower than 0.3 and a standard error of 6.3 %. Analysing in detail the calculated model at the drill-hole position, it is noticeable that most of the layers are well differentiated. The shallow resistive layer of dunes sands and clays is defined with a resistivity higher than 30 Ω·m at 6 m depth. The second resistivity layer (~10 Ω·m) represents sands, clays and the top of biocalcarenites with a thickness of 13 m. Below, the bottom of biocalcarenites is represented with a resistivity of ~5 Ω·m. Finally, from 25 to 40 m depth it is detected a very low resistive layer (~1 Ω·m) that is assigned to the saltwater presence and clays at the top. The bottom of the profile has a resistivity of ~3 Ω·m belonging to karstified limestones, calcareous marl and clays from Miocene.

5. Discussion

5.1 Strengths and weaknesses of resistivity and TDEM geophysical methods and joint inversion

To better characterize an area, the combination of geophysical methods has become increasingly necessary (Garambois *et al.*, 2002; Martínez-Moreno *et al.*, 2013). This is because each geophysical method determines different physical properties underground. The use of a single geophysical method provides partial information (Bauer-Gottwein *et al.*, 2010; Martínez-Moreno *et al.*, 2016), whilst the combination of two or more techniques offers a more complete solution (Meric *et al.*, 2005; Martínez-Moreno *et al.*, 2014). Within the different geophysical methods, based on electrical and electromagnetic methods (both obtain apparent resistivity underground), different results are found depending on the characteristics of each method (Schmutz *et al.*, 2000; Monteiro Santos and El-Kaliouby, 2010). Since resistivity better defines the shallowest areas and is more sensitive to resistive structures, time domain electromagnetic is focused in deeper parts with great sensitivity to conductors (Monteiro Santos *et al.*, 2011; Bortolozo *et al.*, 2015). Both methods are ideally combinable to apply them together (Godio and Bottino, 2001; Schiavone and Valenza, 2010).

Regarding the results of the current study, single inversion of the geophysical methods applied (Fig. 4) provides approximate results of the problem, however some details may be hidden precisely due to the properties measured on each method. In addition, this single inversion of two methods give rise to separate models that must be analysed by comparison in contrast to joint inversion that obtain a single model (Monteiro Santos *et al.*, 2006).

The use of the joint inversion provides a unique model that encompasses physical properties measured on each method. The combination creates a more reliable and fitted results allowing to determine a more robust distribution of the resistivity and, therefore, to better define the subsurface structure and groundwater conditions.

5.2 Advances in 1D joint inversion of DRC and TDEM data

The first inconvenience found when performing joint inversion has been the static shift between VES and TDEM data (Meju, 2005; Bortolozo *et al.*, 2015). There is a phase shift in the curves of the applied methods that should be corrected (Fig. 3). Since the transient method provides more realistic apparent resistivity distribution underground (Srigutomo *et al.*, 2008), the VES curves have been multiplied by a factor to fit with the TDEM curves. The observed phase shift between both methods is usual due to the resistivity method is affected by ground heterogeneities, as well as the measuring electrodes in direct contact with the ground generates perturbations (Bortolozo *et al.*, 2015).

Comparing both the 1D and quasi-2D joint inversion results it has been demonstrated that quasi-2D joint inversion improves the models when compared with the 1D joint inversion. The analysis is based on drill-hole information in profile 2 (Figs.

6 and 8). Whilst in the 1D joint inversion it is only considered each individualised site (Monteiro Santos and El-Kaliouby, 2010) in the quasi-2D joint inversion the data surrounding each cell is taken into account (Monteiro Santos and El-Kaliouby, 2011). If it is assumed that electrical methods are affected by the resistivity of the neighbouring structures, the joint inversion seems to provide more fitted models of resistivity distribution underground due to it make allowances for the data around them.

The quasi-2D joint inversion may also have higher errors than single approaches due to the use of more data in the second inversion uses more data quantity. In addition, resistivity variation in two direction causes more influence in the data causing higher errors. However, both have a standard error around 10% and 6% in profile 1 and 2 respectively, and the calculated DOI index (Oldenburg and Li, 1999; Marescot *et al.*, 2003) indicates that they are trusted. This calculation demonstrates that the profiles are not restricted to the initial model but they are subject to the data.

The applied joint inversion both 1D and quasi-2D have improved the results obtained by the single inversion. In addition, the quasi-2D joint inversion highlights the sedimentary layers revealed in the exploration drilling.

6. Conclusions

Seawater intrusions is a widespread problem detected in coastal aquifers. The actions to mitigate or remediate this problem goes through detect the intrusion. The combined use of resistivity and TDEM methods have been applied to study the seawater intrusion in a coastal area at the S of the Algarve Basin. The study zone has an exploration drilling located at the centre of the profile 2 where different sedimentary layers have been recognised in the geophysical results.

Three different manners of inversion data has been carried out. First, a single inversion of the data in a traditional manner has been performed and the obtained results do not exactly match with the drilling information. However, the areas with saltwater intrusion are highlighted. Secondly, 1D joint inversion of the data was calculated for each profile and the models have improved markedly. The seawater intrusion areas are better defined in this inversion and the surface areas are better delineated. More layers with resistivity contrast are differentiated with respect to the previous inversion regarding to drilling information, however they still do not adjust. Finally, it was performed a quasi-2D joint inversion obtaining better results. These models can differentiate each sedimentary layer registered in the drill-hole (better than single and 1D joint inversion), including morphology and depth.

The models calculated with quasi-2D joint inversion has notably improved the previous data inversions. The location of seawater intrusion is better defined through the quasi-2D joint inversion respect to single and 1D joint inversions. This kind of inversion has multiple applications: minning, hydrogeology or engineering among others. Therefore, it is concluded that the combination of geoelectrical methods improves the results analysis regarding to resistivity distribution underground. Of the three proposed methods the quasi-2D joint inversion offers the most reliable results.

Acknowledgements

Publication supported by project FCT UID/GEO/50019/2013 - Instituto Dom Luiz.

Figure captions

Figure 1: Simplified geological scheme of the aquifer system Ferragudo-Albufeira. The delimitation of the study area is indicated (Modified from Almeida *et al.*, 2004).

Figure 2: Detailed location and distribution of the resistivity profiles and time domain electromagnetic (TDEM) soundings. Drill-hole position and sedimentary sequence are indicated.

Figure 3: Static shift correction of the vertical electrical soundings (VES) curves with regard to time domain electromagnetic (TDEM) ones.

Figure 4: 2D-pseudosection models for single inversion of VES (a, c) and TDEM (b, d) data. Drilling information is displayed over the pseudosection in profile 2.

Figure 5: Curves adjustment for VES and TDEM data obtained from 1D joint inversion.

Figure 6: 2D-pseudosection models obtained from 1D joint inversion of VES and TDEM data. Drilling information is displayed over the pseudosection in profile 2.

Figure 7: Curves adjustment for VES and TDEM data obtained from quasi-2D joint inversion.

Figure 8: 2D-pseudosection models obtained from quasi-2D of VES and TDEM data. DOI index cut-off value is indicated in profile 1, whereas that profile 2 is below that the selected cut-off value. Drilling information is displayed over the pseudosection in profile 2.

REFERENCES

Abdul Nassir, S., Loke, M., Lee, C., Nawawi, M. 2000. Salt-water intrusion mapping by geoelectrical imaging surveys. Geophysical Prospecting, 48, 647-661. doi: 10.1046/j.1365-2478.2000.00209.x

Adepelumi, A.A., Ako, B.D., Ajayi, T.R., Afolabi, O., Omotoso, E.J., 2009. Delineation of saltwater intrusion into the freshwater aquifer of Lekki Peninsula, Lagos, Nigeria. Environmental Geology, 56(5): 927-933. doi:10.1007/s00254-008-1194-3

Almeida, C., Mendonça, J.J.L., Jesus, M.R., Gomes, A.J. 2000. Sistemas aquíferos de Portugal continental. Instituto da Água, Lisbon, Portugal.

Antunes, M., Pais, J. 1992. The Neogene and Quaternary of Algarve. Ciências da Terra (UNL), número especial II, 57-66.

Auken, E., Christiansen, A.V. 2004. Layered and laterally constrained 2D inversion of resistivity data. Geophysics, 69, 752-761. doi: 10.1190/1.1759461

Auken, E., Christiansen, A.V., Jacobsen, B.H., Foged, N., Sørensen, K.I. 2005. Piecewise 1D laterally constrained inversion of resistivity data. Geophysical Prospecting, 53, 497-506. doi: 10.1111/j.1365-2478.2005.00486.x

Bauer-Gottwein, P., Gondwe, B.N., Christiansen, L., Herckenrath, D., Kgotlhang, L., Zimmermann, S. 2010. Hydrogeophysical exploration of three-dimensional salinity anomalies with the time-domain electromagnetic method (TDEM). Journal of Hydrology, 380, 318-329.

Bear, J., Cheng, A.H.-D., Sorek, S., Ouazar, D., Herrera, I. 1999. Seawater intrusion in coastal aquifers: concepts, methods and practices. Springer Science, Business Media.

Bortolozo, C.A., Porsani, J.L., Santos, F.A.M.d., Almeida, E.R. 2015. VES/TEM 1D joint inversion by using Controlled Random Search (CRS) algorithm. Journal of Applied Geophysics, 112, 157-174, doi: http://dx.doi.org/10.1016/j.jappgeo.2014.11.014.

Calvache, M.L., Pulido-Bosch, A. 1994. Modeling the Effects of Salt-Water Intrusion Dynamics for a Coastal Karstified Block Connected to a Detrital Aquifer. Groundwater, 32, 767-777.

Custodio, E. 1987. Prediction methods. Chapter 8. Studies and reports in hydrology: groundwater problems in coastal areas. United Nations Educational, Scientific and Cultural Organization, Paris.

Duque, C., Calvache, M.L., Pedrera, A., Martín-Rosales, W., López-Chicano, M. 2008. Combined time domain electromagnetic soundings and gravimetry to determine marine intrusion in a detrital coastal aquifer (Southern Spain). Journal of Hydrology, 349, 536-547, doi: 10.1016/j.jhydrol.2007.11.031.

El-Kaliouby, H., Abdalla, O. 2015. Application of time-domain electromagnetic method in mapping saltwater intrusion of a coastal alluvial aquifer, North Oman. Journal of Applied Geophysics, 115, 59-64, doi: 10.1016/j.jappgeo.2015.02.003.

Everett, M.E. 2013. Near-surface applied geophysics. Cambridge University Press. doi: 10.1017/CBO9781139088435

Fainberg, E. 1999. TEM-Fast 48 manual. Amsterdam, The Netherlands: Applied Electromagnetic Research.

Francés, A.P., Ramalho, E.C., Fernandes, J., Groen, M., De Plaen, J., Hugman, R., Khalil, M.A., Monteiro-Santos, F.A. 2014. Hydrogeophysics contribution to the development of hydrogeological conceptual model of coastal aquifers–Albufeira-Ribeira de Quarteira aquifer case study. proceedings of: 8ª Assembleia Luso Espanhola de Geodesia e Geofísica.

Garambois, S., Sénéchal, P., Perroud, H. 2002. On the use of combined geophysical methods to assess water content and water conductivity of near-surface formations. Journal of Hydrology, 259, 32-48, doi: 10.1016/S0022-1694(01)00588-1.

Godio, A., Bottino, G. 2001. Electrical and electromagnetic investigation for landslide characterisation. Physics and Chemistry of the Earth, Part C: Solar, Terrestrial, Planetary Science, 26, 705-710, doi: 10.1016/S1464-1917(01)00070-8.

Kazakis, N., Pavlou, A., Vargemezis, G., Voudouris, K., Soulios, G., Pliakas, F., Tsokas, G. 2016. Seawater intrusion mapping using electrical resistivity tomography and hydrochemical data. An application in the coastal area of eastern Thermaikos Gulf, Greece. Science of the Total Environment, 543, 373-387, doi: 10.1016/j.scitotenv.2015.11.041.

Khalil, M.A., Monteiro Santos, F.A. 2013. 2D and 3D resistivity inversion of Schlumberger vertical electrical soundings in Wadi El Natrun, Egypt: A case study. Journal of Applied Geophysics, 89, 116-124, doi: 10.1016/j.jappgeo.2012.11.014.

Knight, J., Raiche, A. 1982. Transient electromagnetic calculations using the Gaver-Stehfest inverse Laplace transform method. Geophysics, 47, 47-50, doi: 10.1190/1.1441280.

Loke, M.H. 2016. Tutorial: 2-D and 3-D Electrical Imaging Surveys. Geotomo Software Company.

Lopes, F.C., Cunha, P.P., Le Gall, B. 2006. Cenozoic seismic stratigraphy and tectonic evolution of the Algarve margin (offshore Portugal, southwestern Iberian Peninsula). Marine Geology, 231, 1-36, doi: 10.1016/j.margeo.2006.05.007.

Manuppella, G. 1992. Carta geológica da região do Algarve, escala 1/100 000. Serv. Geol. Portugal.

Marescot, L., Loke, M.H., Chapellier, D., Delaloye, R., Lambiel, C., Reynard, E. 2003. Assessing reliability of 2D resistivity imaging in mountain permafrost studies using the depth of investigation index method. Near Surface Geophysics, 1, 57-67, doi: 10.3997/1873-0604.2002007

Martínez-Moreno, F.J., Galindo-Zaldívar, J., Pedrera, A., Teixido, T., Ruano, P., Peña, J.A., González-Castillo, L., Ruiz-Constán, A., López-Chicano, M., Martín-Rosales, W. 2014. Integrated geophysical methods for studying the karst system of Gruta de las Maravillas (Aracena, Southwest Spain). Journal of Applied Geophysics, 107, 149-162, doi: 10.1016/j.jappgeo.2014.05.021.

Martínez-Moreno, F.J., Monteiro-Santos, F.A., Madeira, J., Bernardo, I., Soares, A., Esteves, M., Adão, F. 2016. Water prospection in volcanic islands by Time Domain Electromagnetic (TDEM) surveying: The case study of the islands of Fogo and Santo Antão in Cape Verde. Journal of Applied Geophysics, 134, 226-234, doi: 10.1016/j.jappgeo.2016.09.020.

Martínez-Moreno, F.J., Pedrera, A., Ruano, P., Galindo-Zaldívar, J., Martos-Rosillo, S., González-Castillo, L., Sánchez-Úbeda, J.P., Marín-Lechado, C. 2013. Combined microgravity, electrical resistivity tomography and induced polarization to detect deeply buried caves: Algaidilla cave (Southern Spain). Engineering Geology, 162, 67-78, doi: 10.1016/j.enggeo.2013.05.008.

Meju, M.A. 2002. Geoelectromagnetic exploration for natural resources: models, case studies and challenges. Surveys in Geophysics, 23, 133-206, doi: 10.1023/A:1015052419222.

Meju, M.A. 2005. Simple relative space–time scaling of electrical and electromagnetic depth sounding arrays: implications for electrical static shift removal and joint DC-TEM data inversion with the most-squares criterion. Geophysical Prospecting, 53, 463-479, doi: 10.1111/j.1365-2478.2005.00483.x.

Meric, O., Garambois, S., Jongmans, D., Wathelet, M., Chatelain, J.-L., Vengeon, J. 2005. Application of geophysical methods for the investigation of the large gravitational mass movement of Séchilienne, France. Canadian Geotechnical Journal, 42, 1105-1115, doi: 10.1139/T05-034.

Monteiro Santos, F.A. 2004. 1-D laterally constrained inversion of EM34 profiling data. Journal of Applied Geophysics, 56, 123-134, doi: 10.1016/j.jappgeo.2004.04.005.

Monteiro Santos, F.A., Dupis, A., Afonso, A.R.A., Victor, L.A.M. 1997. 1D joint inversion of AMT and resistivity data acquired over a graben. Journal of Applied Geophysics, 38, 115-129, doi: 10.1016/S0926-9851(97)80020-1.

Monteiro Santos, F.A., El-Kaliouby, H.M. 2010. Comparative study of local versus global methods for 1D joint inversion of direct current resistivity and time-domain electromagnetic data. Near Surface Geophysics, 8, 135-143, doi: 10.3997/1873-0604.2009056.

Monteiro Santos, F.A., Trota, A., Soares, A., Luzio, R., Lourenço, N., Matos, L., Almeida, E., Gaspar, J.L., Miranda, J.M. 2006. An audio-magnetotelluric investigation in Terceira Island (Azores). Journal of Applied Geophysics, 59, 314-323, doi: 10.1016/j.jappgeo.2005.12.001.

Monteiro-Santos, F.A., El-Kaliouby, H.M. 2011. Quasi-2D inversion of DCR and TDEM data for shallow investigations. Geophysics, 76, F239-F250, doi: 10.1190/1.3587218.

Nabighian, M.N. 1988. Electromagnetic methods in applied geophysics. SEG Books.

Nguyen, F., Kemna, A., Antonsson, A., Engesgaard, P., Kuras, O., Ogilvy, R., Gisbert, J., Jorreto, S., Pulido-Bosch, A. 2009. Characterization of seawater intrusion using 2D electrical imaging. Near Surface Geophysics, 7, 377-390, doi: 10.3997/1873-0604.2009025.

Nicaise, Y., Marc, D., Michel, V.J., Christian, A. 2013. Delimitation of the Salt Water Wedge in the Shallow Coastal Aquifer by TDEM Method at Togbin (South Benin). International Journal of Science and Advanced Technology.

Oldenburg, D.W., Li, Y. 1999. Estimating depth of investigation in dc resistivity and IP surveys. Geophysics, 64, 403-416, doi: 10.1190/1.1444545.

Raiche, A., Jupp, D., Rutter, H., Vozoff, K. 1985. The joint use of coincident loop transient electromagnetic and Schlumberger sounding to resolve layered structures. Geophysics, 50, 1618-1627, doi: 10.1190/1.1441851.

Rey, J. 1983. Le Crétacé de l'Algarve: Essai de synthèse. Comunicações dos Serviços Geológicos de Portugal, 69, 8.

Schiavone, S., Valenza, M. 2010. Integrated hydrogeochemical and geophysical surveys for a study of sea-water intrusion. Bollettino di Geofisica Teorica ed Applicata, 51, 285-300.

Schmutz, M., Albouy, Y., Guérin, R., Maquaire, O., Vassal, J., Schott, J.-J., Descloîtres, M. 2000. Joint electrical and time domain electromagnetism (TDEM) data inversion applied to the Super Sauze earthflow (France). Surveys in Geophysics, 21, 371-390, doi: 10.1023/A:1006741024983.

Sherif, M., Mahmoudi, A.E., Garamoon, H., Kacimov, A., Akram, S., Ebraheem, A., Shetty, A. 2006. Geoelectrical and hydrogeochemical studies for delineating seawater intrusion in the outlet of Wadi Ham, UAE. Environmental Geology, 49, 536-551, doi: 10.1007/s00254-005-0081-4.

Sherif, M.M., Singh, V.P. 1999. Effect of climate change on sea water intrusion in coastal aquifers. Hydrological Processes, 13, 1277-1287, doi: 10.1002/(SICI)1099-1085(19990615)13:8<1277::AID-HYP765>3.0.CO;2-W.

Simancas, J. 2004. Zona Sudportuguesa. In: Geología de España. SGE-IGME, Madrid, 199-201.

Song, S.-H., Lee, J.-Y., Park, N., 2007. Use of vertical electrical soundings to delineate seawater intrusion in a coastal area of Byunsan, Korea. Environmental Geology, 52(6): 1207-1219. doi:10.1007/s00254-006-0559-8

Srigutomo, W., Kagiyama, T., Kanda, W., Munekane, H., Hashimoto, T., Tanaka, Y., Utada, H., Utsugi, M. 2008. Resistivity structure of Unzen Volcano derived from time domain electromagnetic (TDEM) survey. Journal of volcanology and geothermal research, 175, 231-240, doi: 10.1016/j.jvolgeores.2008.03.033.

Viezzoli, A., Christiansen, A.V., Auken, E., Sørensen, K. 2008. Quasi-3D modeling of airborne TEM data by spatially constrained inversion. Geophysics, 73, F105-F113, doi: 10.1190/1.2895521.

Vozoff, K., Jupp, D. 1975. Joint inversion of geophysical data. Geophysical Journal International, 42, 977-991, doi: 10.1111/j.1365-246X.1975.tb06462.x.

Ward, S.H., Hoekstra, P., Blohm, M.W. 1990. Case Histories of Time-Domain Electromagnetic Soundings in Environmental Geophysics. Geotechnical an Environmental Geophysics. Society of Exploration Geophysicists, 1-16.

Werner, A.D., Bakker, M., Post, V.E., Vandenbohede, A., Lu, C., Ataie-Ashtiani, B., Simmons, C.T., Barry, D.A. 2013. Seawater intrusion processes, investigation and management: recent advances and future challenges. Advances in Water Resources, 51, 3-26, doi: 10.1016/j.advwatres.2012.03.004.

Werner, A.D., Gallagher, M.R. 2006. Characterisation of sea-water intrusion in the Pioneer Valley, Australia using hydrochemistry and three-dimensional numerical modelling. Hydrogeology Journal, 14, 1452-1469, doi: 10.1007/s10040-006-0059-7.

Figure_1
Click here to download high resolution image

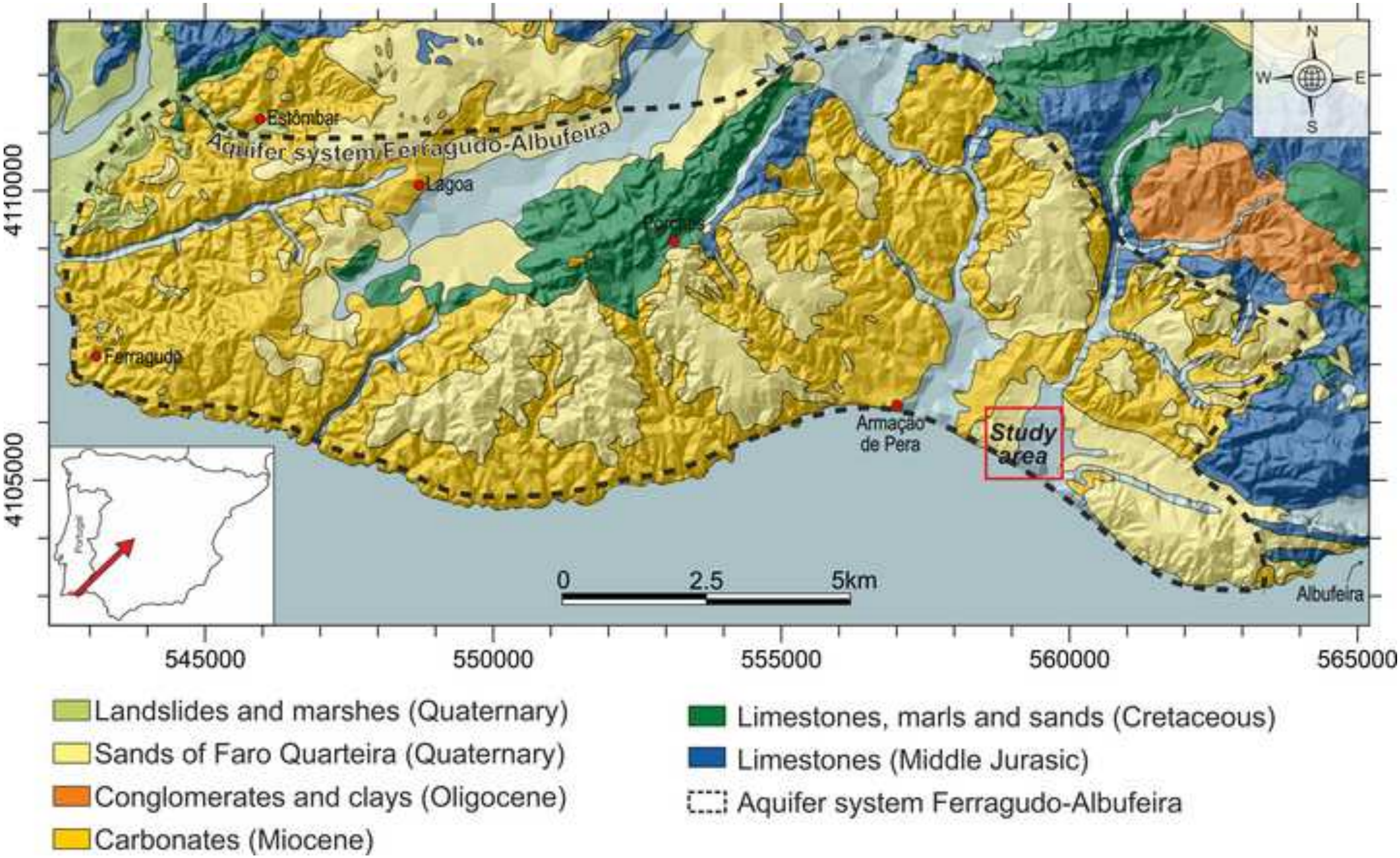

Figure_2

Click here to download high resolution image

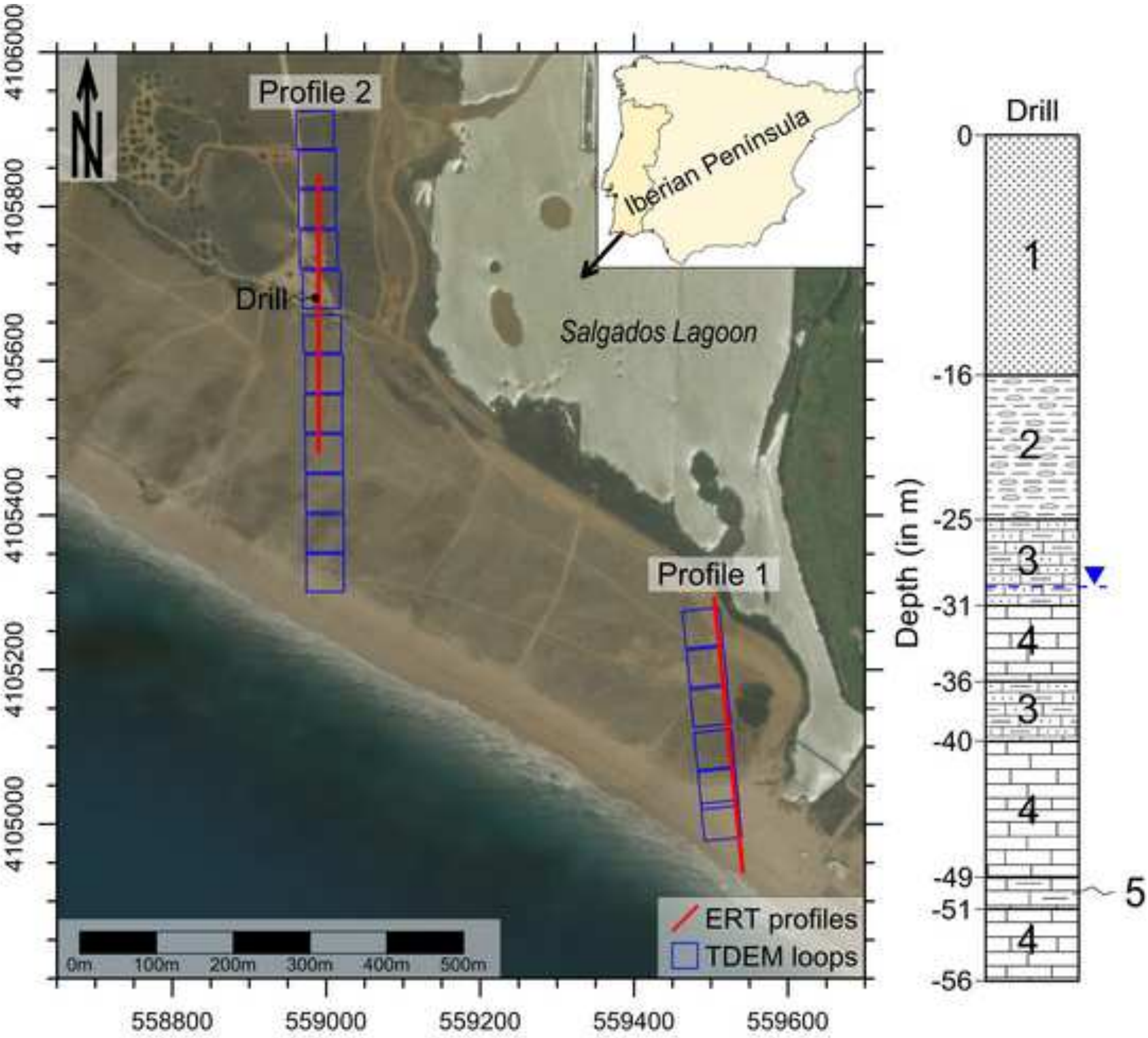

Statigraphic Column

1 – Sands and clays (Quaternary)

2 – Biocalcarenites (Miocene)

3 – Marly limestones and clays (Miocene)

4 – Karstified limestones (Miocene)

5 – Calcareous marl and clays (Miocene)

Figure_3
Click here to download high resolution image

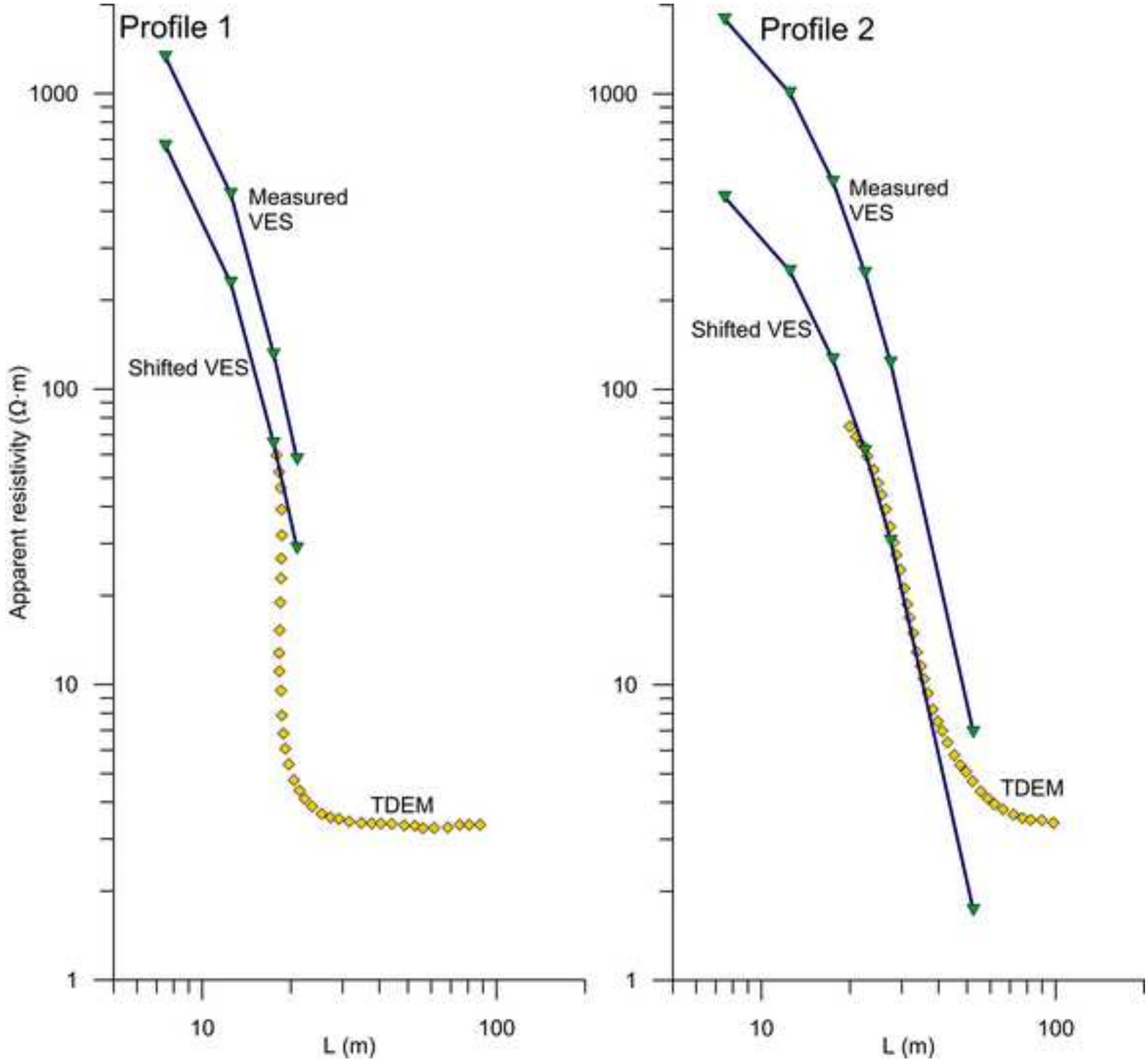

Figure_4

Click here to download high resolution image

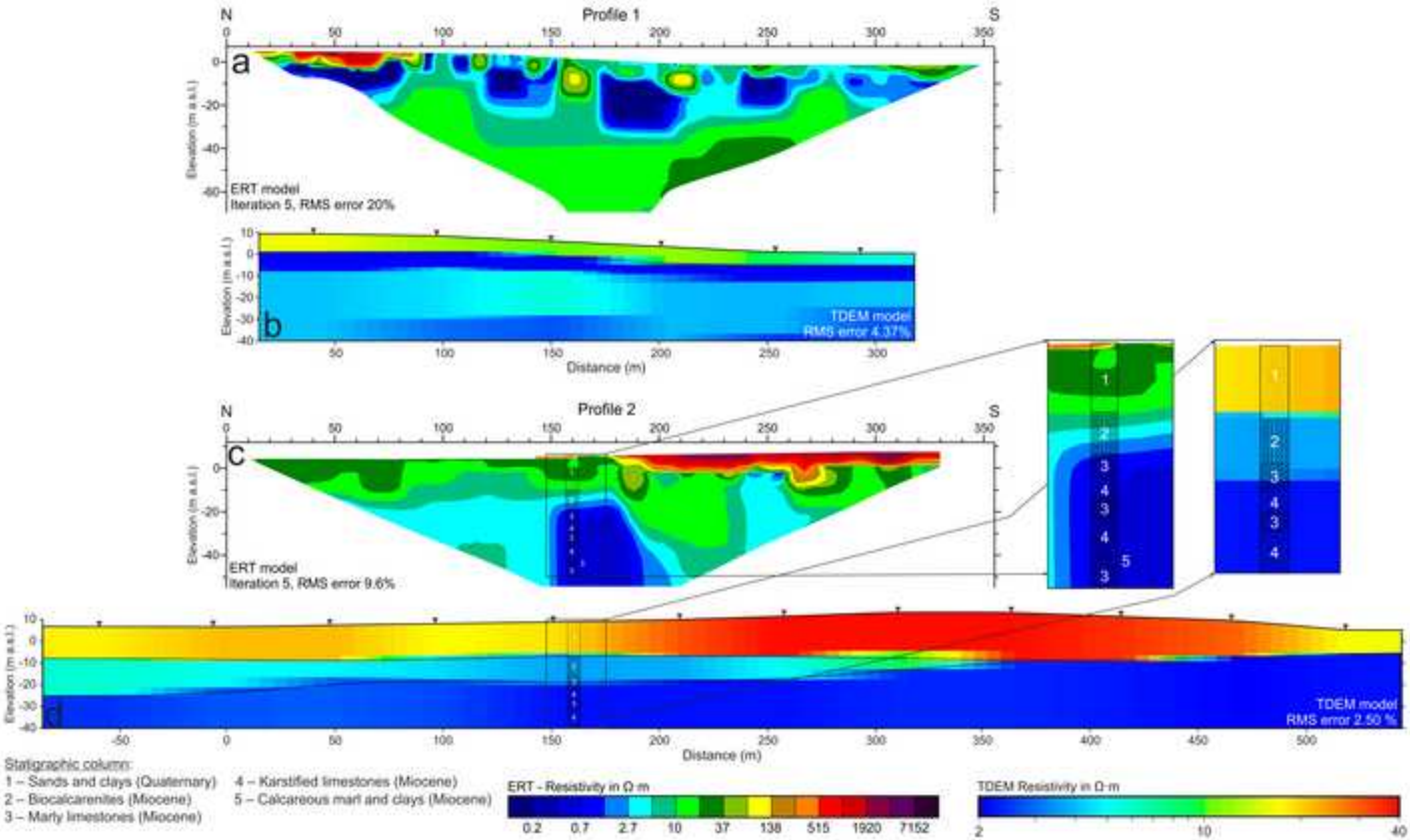

Figure_5
Click here to download high resolution image

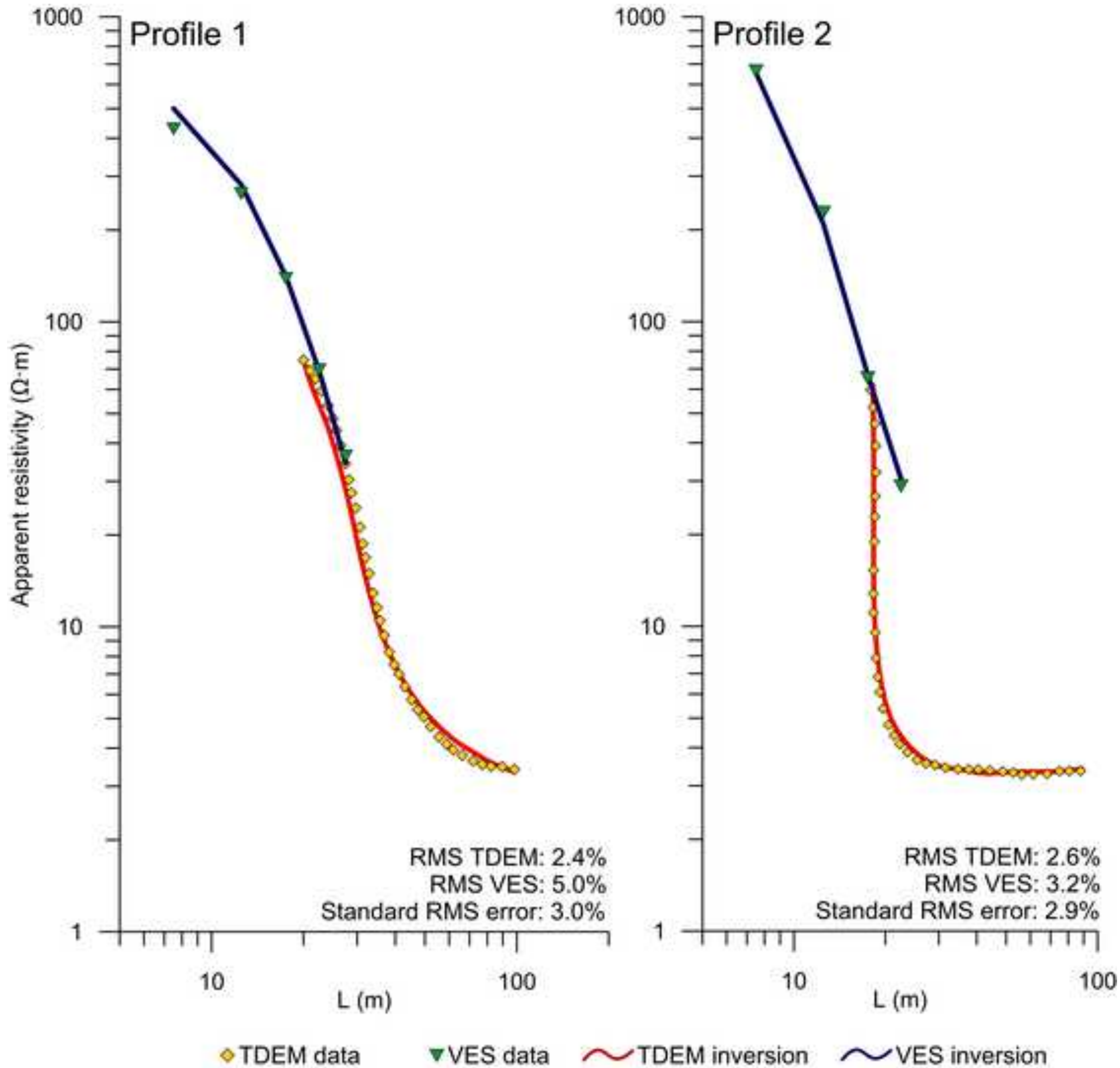

Figure_6
Click here to download high resolution image

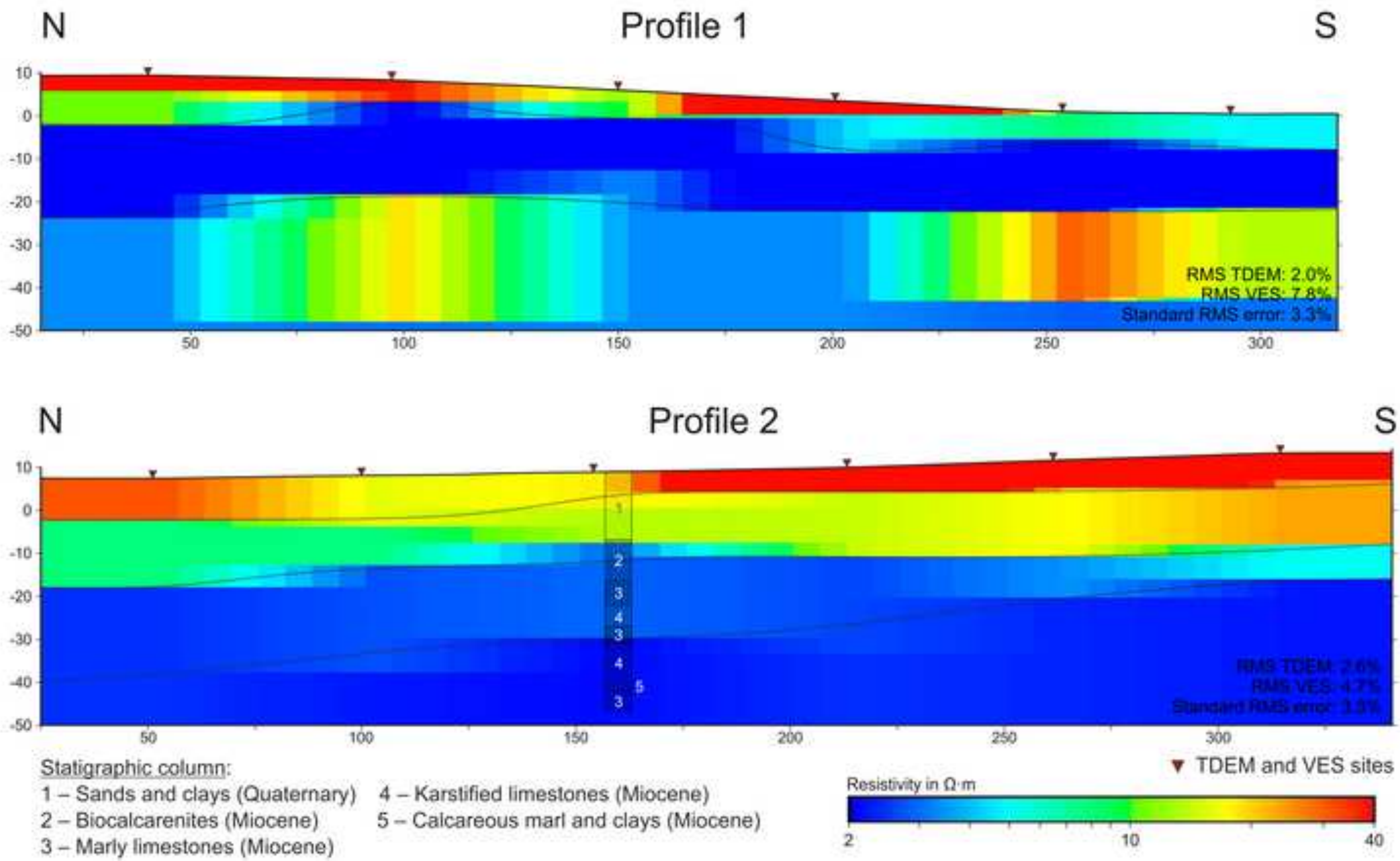

Figure_7

Click here to download high resolution image

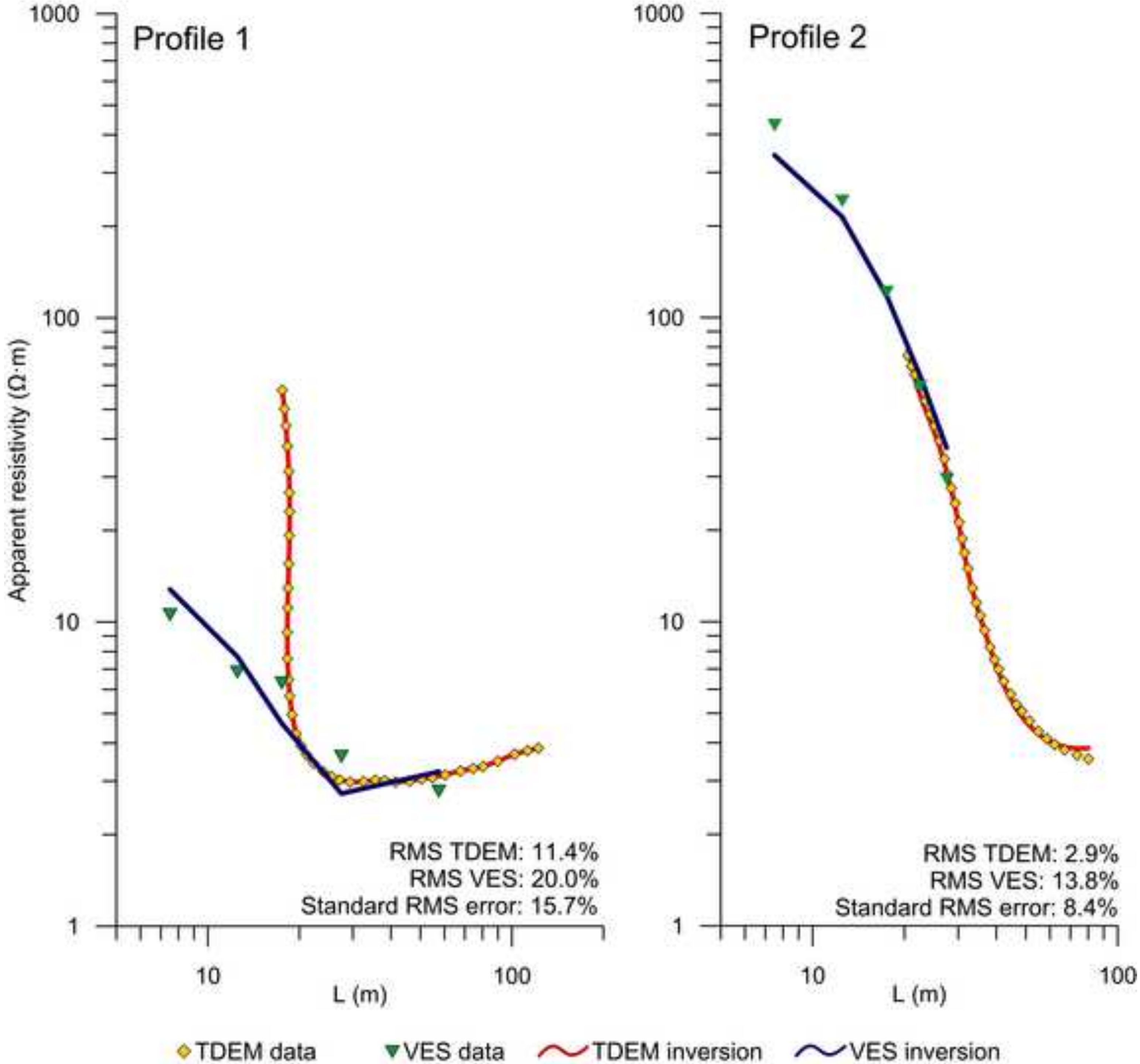

Figure_8
Click here to download high resolution image